RSC Sustainability

ROYAL SOCIETY OF CHEMISTRY

PAPER

View Article Online
View Journal | View Issue

Cite this: *RSC Sustainability*, 2023, **1**, 2305

A novel shape-stabilized phase change material with tunable thermal conductivity for cold chain applications

Prakhar Dixit,[ab] Apoorv Balwani,[c] Tridib Ambardar,[c] Vennapusa Jagadeeswara Reddy,[ad] Tushar Kanti Maiti,[ae] Adarsh Kumar Pandey,[f] Aravind Dasari*[b] and Sujay Chattopadhyay*[a]

Phase change materials (PCMs) are popular in cold-chain logistics as evidenced by the commercial success of various PCM-based thermal shippers. Improvement in the thermal performance of PCMs can improve their sustainability and viability. Herein, a novel, thermally conductive PCM composite is evaluated for transporting thermally sensitive perishables in the temperature window of −14 °C to 25 °C. The PCM (OH-64), developed from a eutectic mixture of a commercial PCM and hexadecane, was found to have a melting temperature of 6.87 °C and crystallization onset at 4.86 °C. Expanded graphite (EG) was added to improve the shape stability and reduce the activation time. The thermal characterization of OH-64 indicated no significant changes in the melting/crystallization temperature after the addition of 11.1 wt% EG and resulted in only a 5% decrease in fusion enthalpy as compared to the original blend. The composite's thermal conductivity dependence on the bulk density suggests that this property may be tuned by changing the morphology of the resulting composites. The applicability of OH-64 was evaluated by incorporating it into a thermal shipper with a chocolate payload and subjecting the box to different ambient temperatures. The thermal buffering effect of the composite was significant despite the absence of thermal insulation. Thus, the OH-64 eutectic PCM composite prepared in this study would be potentially useful for low-temperature thermal buffering applications in cold-chain food and pharmaceutical logistics.

Received 19th August 2023
Accepted 15th October 2023

DOI: 10.1039/d3su00289f

rsc.li/rscsus

Sustainability spotlight

The utilization of thermal energy storage systems that integrate eutectic phase change materials with improved thermal conductivity is an extremely effective means of storing thermal energy owing to various advantages, such as the ability to store significant amounts of energy, a broad range of operating temperatures, a straightforward synthesis process, and the potential for clean energy storage and supply. Improving the thermal properties of eutectic phase change material systems can lead to significant technological advancements in thermal shipping boxes, resulting in improved sustainability, reusability, and cost-effectiveness over the long term. Therefore, this article presents a new method of creating eutectic phase change material composites, and the resulting composite has demonstrated great efficiency for low-temperature thermal buffering applications, specifically in cold-chain logistics for food and pharmaceuticals. The development of such eutectic phase change material composites is in line with the Sustainable Development Goals of the UN, which aim to achieve affordable and sustainable energy storage and act against climate change.

1. Introduction

Recently, cold chain logistics has gained much interest from the thermal management community, particularly due to rising pressures on sustainable practices, the increased demand for fresh items, and the emphasis on the safe and economical delivery of food and pharmaceutical supplies, which is recently seen with the rise of COVID-19.[1–3] According to studies, improper temperature storage and transportation results in a third of the fresh foods consumed worldwide being wasted. The effective utilization of the cold chain, particularly in the transportation of thermally sensitive perishables, such as food

[a]*Polymer and Process Engineering, IIT Roorkee Saharanpur Campus, Saharanpur-247001, India. E-mail: sujay@pe.iitr.ac.in*

[b]*School of Material Science and Engineering, Nanyang Technological University, 50 Nanyang Avenue, Singapore 639798. E-mail: aravind@ntu.edu.sg*

[c]*New Product Initiatives, R&D, Pluss Advance Technologies Pvt. Ltd., Gurgaon-122003, India*

[d]*Center for Advanced Research in Fluid Flow (CARIFF), University of Malaysia Pahang, Malaysia*

[e]*Department of Chemical Engineering, University of Bath, Claverton Down, BA2 7AY, UK*

[f]*Research Center for Nano-materials and Energy Technology (RCNMET), School of Engineering and Technology, Sunway University, No. 5, Jalan Universiti, Bander Sunway, Petaling Jaya, Selangor Darul Ehsan, 47500, Malaysia*

and vaccines, is pertinent to solving this problem.[4–6] However, the cold chain industry is heavily reliant on fossil fuels to fulfil cooling requirements during the transit. Thermal energy storage solutions/systems (TESS) can be used to store energy offsite and employed *ad hoc* as portable thermal logistics solutions, thus reducing cooling loads on transport media and improving last-mile portability.[7,8] Phase change materials (PCMs) have enabled TESS to benefit from high energy storage density and low cost per unit weight, reducing the volumetric and gravimetric payload requirements during cold chain transport and the need for fossil fuels.[9–11] As a result, PCM-based TESS are becoming a popular alternative for improving access to non-conventional energy sources with intermittent supply and access to precise thermal control in mobility solutions.[12–14]

Eutectic PCMs are a mixture of organic–organic, organic–inorganic, or inorganic–inorganic PCMs. These PCMs are tailor-made by blending two or more PCMs to achieve a unique PCM of distinct, singular melting and crystallization temperatures, different from the constituent PCMs.[15–17] While eutectics have been traditionally developed by trial and error, some research groups have also employed thermodynamic calculations to predict the melting point depression in different PCMs to elucidate their combined eutectic behavior (*e.g.*, the Schrader equation and Gibbs–Thomson equation).[18,19] In any case, much of the PCM discoveries in the last decade can be attributed to studies in eutectic mixtures. Liu *et al.*[20] prepared a eutectic hydrated salt by mixing $Na_2CO_3 \cdot 10H_2O$ and $Na_2HPO_4 \cdot 12H_2O$ in a mass ratio of 40 : 60. The prepared eutectic had a latent heat of 220.2 J g^{-1} and phase change temperature of 27.3 °C, and was found to be a good contender for applications related to building thermal control. Chinnasamy and coworkers[21] prepared a eutectic blend by mixing 40 wt% lauric acid and 60 wt% myristyl alcohol, with a resulting phase change temperature of 21.3 °C and latent heat of 151.6 J g^{-1}. The blend was found to be thermally stable for up to 1000 cycles. Li *et al.*[16] prepared a eutectic organic–inorganic mixture of $Mg(NO_3)_2 \cdot 6H_2O$ (MNH) and glutaric acid (GA) with a composition of 60 wt% MNH and 40 wt% GA. Interestingly, the eutectic PCM's enthalpy was higher than the individual PCMs, which is attributed to the crystalline transformation of the eutectic that was potentially facilitated by the hydrogen bonds between MNH and GA. A melting temperature of 66.7 °C and a melting enthalpy of 189 J g^{-1} were displayed by the prepared eutectic. To the best of the authors' knowledge, most of the eutectic PCMs reported in the literature have functional temperature ranges that are suitable for building envelope and solar energy storage applications. At the same time, there have been very few studies on eutectic mixtures for cooling/freezing application domains.[22–29]

The primary disadvantage of traditional PCMs (including eutectic mixtures) is their tendency to leak and flow in their liquid state.[30,31] The use of containers and bulk encapsulants levy a constraint on the portability of the PCM-enabled TESS design, particularly in last-mile transport/delivery applications. Encapsulating PCMs at the micro- and nano-scales (core–shell encapsulation) and entrapping PCMs within highly networked matrices and foams to create shape-stabilized composites could solve this issue.[32–36] The core–shell approach is described as difficult, costly, and energy-intensive, making it commercially unviable.[35,37] On the other hand, shape-stabilized PCM rose to prominence due to a simple production technique, as well as efficient performance, easy scalability, and affordability.[8,38,39] Shape stabilization of PCMs is a dependable approach to giving organic PCMs a leg up by eliminating their containment issues and enabling easy additive incorporation for improved composite properties.[40,41] Due to its wide surface area, high crystallinity, superior thermal conductivity, lipophilicity, and high aspect ratio, a graphite-based supporting matrix is thought to be an appropriate material for producing a shape-stabilized PCM. Expanded graphite (EG)[42–45] is a well-known carbonaceous material that has a high conductivity and a porous worm-like structure that prevents leaking of organic PCMs by virtue of van der Waals interactions and the capillary effect. Entrapping PCMs in these materials has been the subject of many recent studies. Alkhazaleh *et al.*[46] prepared a eutectic system using 80% butyl stearate and 20% isopropyl palmitate and impregnated EG with it. In the composite preparation, 90% PCM eutectic and 10% EG were used. The addition of EG enhanced the thermal conductivity by 58.3%. The prepared eutectic composite showed melting between 15–19 °C with a latent heat of fusion of 119 J g^{-1}. The prepared PCM composite reduced the inner temperature of the room by 1.6 °C and provided thermal comfort in building the envelope. Liu *et al.*[47] prepared a decyl alcohol–lauric acid eutectic and impregnated EG with it by vacuum adsorption method, with a 2.08 °C melting temperature and latent heat of 188.71 J g^{-1}. In the composite, the mass ratio of PCM and EG was found to be 12 : 1, and the thermal conductivity of the PCM composite was enhanced by 13.75 times as compared to PCM. After 500 heating and cooling cycles, the phase change temperature and enthalpy of the eutectic composite were changed by 5.29% (decreased) and 4.02% (lower). These changes are within the acceptable range. However, the phase transition time increased after thermal cycles because the heat conduction grids inside the eutectic composite were damaged due to multiple cycles, which caused the flagging of the heat exchange performance of the composite. The prepared eutectic composite showed remarkable potential for remitting the vaccine cold chain logistics gap. Moreover, Du *et al.*[48] prepared a eutectic composite of capric–stearic- and palmitic acids with EG in a mass ratio of 12 : 1 by vacuum impregnation. The addition of EG enhanced the thermal conductivity of the PCM by 340%. The prepared eutectic composite showed a melting temperature of 25.39 °C with a melting latent heat of 140.22 J g^{-1}. The latent heat was found to be higher than the theoretically estimated enthalpy, and the authors attributed this to the synergistic effects that EG brings to the composite by reducing the loss of fatty acids due to degradation or volatilization. The addition of EG to PCM may help overcome the leakage problem of the solid–liquid PCM during the phase change, reduce the period of heat storage and release by improving its thermal conductivity, and improve thermal stability.[49]

The primary goal of this report is to make an EG-based eutectic PCM composite with a low melting point (between 0 °C and 10 °C) that can be used to transport temperature-sensitive products such as COVID vaccines, chocolates, and other foods, as well as to perform detailed thermal and chemical characterizations for potential applications. Since the performance of PCM-based thermal shipping boxes depends upon an interplay of the thermal insulating performance and thermal buffering performance of the shipper boxes, the uniquely "malleable" powder form of the OH-64 composite was also evaluated for heat transfer performance characteristics. For the very first time, a eutectic PCM blend targeted for applications involving the transport of frozen/cooled chocolates was designed and developed using a commercially available fatty acid PCM (OM 18). Binary mixtures of OM-18 and hexadecane were prepared by ultrasonication. A composition of 60 wt% OM-18 and 40 wt% hexadecane exhibited optimal eutectic behavior in the target temperature window, based on DSC performance, and was denoted OH-64. The eutectic equation enabled the discovery and optimization of the mixture. Further, the optimized eutectic PCM was impregnated into EG to make a shape-stabilized composite (OH-64 composite). The dependence of the composite's thermal conductivity on the bulk density suggests a window of tailorable thermal conductivity, which may be tuned by changing the resulting composites' morphology and bulk density. While EG has been previously investigated in PCMs for the enhancement of thermal conductivity, to the best of the authors' knowledge, most of these papers pertain to forming dispersions of graphene/EG in PCM liquids. On the other hand, in this study, the powdered EG worms were utilized as porous matrices to shape-stabilize PCMs. The thermal, chemical, and microstructural properties were characterized by differential scanning calorimetry (DSC), thermal gravimetric analysis (TGA), transient line heat source method (for thermal conductivity), Fourier transform infrared spectroscopy (FTIR), and field emission scanning electron microscopy (FESEM). The stability over multiple thermal cycles was evaluated using repeated thermal cycling across the phase change temperature of the composite. In addition, the temperature-controlled box (TCB), which can maintain the necessary temperature range, was used to test the application ability of the OH-64 composite by deploying along walls utilizing LDPE packets.

2. Experimental section

2.1. Materials

Since eutectic mixtures exhibit mutually suppressed melting points of the constituent PCMs, OM 18 and hexadecane were chosen in this study due to their organic nature, high enthalpy, absence of supercooling, and most importantly, their vicinity to the target payload temperature range (−14 °C to 25 °C). Commercial PCM OM 18, a mixture of fatty acids (melting point: 16.15 °C; enthalpy: 140.72 J g^{-1}) used in this report, was obtained from M/s Pluss Adv. Technologies Pvt. Ltd., India. Hexadecane (melting point: 17.92 °C; enthalpy: 206.46 J g^{-1}) was purchased from M/s Sigma Aldrich, USA. The porous support material, Expandable Graphite, was procured from M/s Tirupati Specialty Graphite, India.

2.2. Other items

Locally purchased items included a temperature monitor with K-type thermocouples and a single wall fiberboard corrugated box. The fiber box had a wall thickness of 2.0 mm, including the corrugation, and had external measurements ($L \times W \times H$) of ($0.126 \times 0.118 \times 0.091$) m. The box was utilized as the TCB for the analysis of the eutectic PCM composite charging and discharging performance as well as its application research. The thermal buffering experiment was carried out using three 80 g Cadbury Bourneville chocolates that were obtained from a neighboring shop.

2.3. Preparation of eutectic OH-64 PCM

Potential eutectic PCM candidates were prepared *via* ultrasonic blending with a succession of weight fractions of OM-18 and hexadecane. In this way, 20 g portions of different samples were prepared, with weight percentages of OM 18 and hexadecane in each sample, as shown in Table 1.

To ensure the appropriate mixing of the PCM constituents in the molten state, the measured weight of OM-18 was first taken in a beaker placed over a hot plate at 30 °C with magnetic stirring. To obtain the desired composition, hexadecane was gradually added while constantly stirring at 500 rpm (using a magnetic bead). The sample was stirred for 20 min at 30 °C, followed by probe sonication for 15 min, before thermal, physicochemical, and performance investigations of the PCM compositions to find the optimal eutectic composition (Fig. 1).

2.4. Preparation of expanded graphite

The expandable graphite was initially subjected to high-temperature drying at 105 °C for 24 h to eliminate the absorbed moisture from its pores. For expansion/exfoliation, these dried samples were heated in a household microwave oven for one minute at various powers, *i.e.*, 100 W, 250 W, 440 W, 715 W, and 900 W. The optimal expansion of expandable graphite occurred

Table 1 Different OM 18 and hexadecane samples for the preparation of eutectic PCMs

Sample name	OM 18 weight (%)	Hexadecane weight (%)
OM 18	100%	—
OH 91	90%	10%
OH 82	80%	20%
OH 73	70%	30%
OH-64	60%	40%
OH 55	50%	50%
OH 46	40%	60%
OH 37	30%	70%
OH 28	20%	80%
OH 19	10%	90%
Hexadecane	—	100%

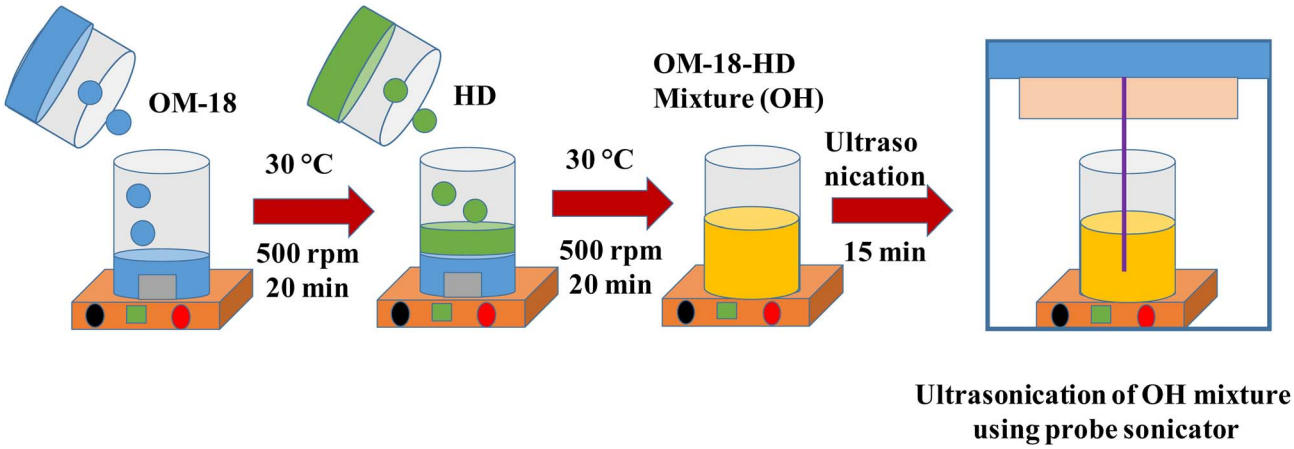

Fig. 1 Schematic representation of the preparation of eutectic PCM OH-64 using OM-18 and hexadecane.

with a dosing power of 900 W. This led to the creation of a noteworthy expanded graphite matrix (EG).[2]

2.5. EG-PCM composite preparation and optimization

Several EG-PCM composite samples were prepared by impregnating different amounts of the resultant EG matrix with a consistent mass of the optimized eutectic PCM formulation. Each of the five beakers, which contained 10 g of eutectic PCM, was heated to a temperature that was 30 °C higher than the material's melting point. The molten eutectic PCM in each sample beaker, labeled sample 1 to sample 5, was gradually supplemented with 1 g, 1.25 g, 1.5 g, 1.75 g, and 2 g EG, respectively. To ensure proper absorption of the eutectic PCM, this mixture was gently stirred for 30 minutes using a glass rod. The eutectic PCM residue was removed from the EG surface by heating these samples to 60 °C for a day. Following this, a leakage test, as prescribed by Dixit and coworkers,[2] was used to determine the optimal mass ratio of EG to PCM for a leak-proof PCM composite, which was found to be about 1.25 : 10.

2.6. Characterization of the eutectic PCM composite

To elucidate PCM sequestration in the porous structure of expanded graphite, surface micrographs of expanded graphite as well as the EG-PCM composite were obtained using a field emission scanning electron microscope (MIRA3, TESCAN). The images were taken at accelerated potentials of 7–10 kV and high vacuum (10^{-10} to 10^{-12} bar). The thermal characteristics of PCM mixture samples during phase transitions were assessed *via* a differential scanning calorimeter (DSC, Discovery DSC25, TA Instruments) under a nitrogen atmosphere. For DSC analysis, approximately 5 mg of samples were taken every time. All samples underwent a minimum of three heating/cooling cycles between −10 °C and 25 °C at a constant heating rate of 5 °C min^{-1}. For analysis and comparison, only the second cycle's data was considered. These results identified the optimized eutectic PCM and further analyzed it using DSC at a heating/cooling rate of 0.5 °C min^{-1} for two cycles (isothermal breaks of 2 minutes were programmed at the beginning of each heating/cooling cycle) to accurately determine its thermal properties. Further, the optimized eutectic blend, OH-64, was evaluated for its thermal stability by continuously cycling the DSC samples between −10 °C to 25 °C at a rate of 5 °C min^{-1} for a hundred cycles. Fourier transformation infrared spectroscopy (FTIR, PerkinElmer FTIR C91158) was used to elucidate the chemical composition in the wavenumber range of 500–4000 cm^{-1}. The thermal conductivities of the optimized eutectic blend, as well as the composite of the eutectic mixture with exfoliated graphite, were characterized by using a transient line source method (KD2 Pro thermal conductivity analyzer), wherein the samples were prepared by filling in a cylindrical tube (diameter = 120 mm) and equilibrating under testing conditions for 15 minutes after the placement of the sensor needle in the center of the cylindrical sample. Both the OH-64 and OH-64 composite were tested at room temperature and subzero temperatures (between −10 °C and −30 °C) to obtain liquid and solid phase thermal conductivity, respectively. For liquid state measurements in OH-64, the KS-1 sensor (single needle, 6 cm) was employed, while all other tests were conducted with the TR-1 sensor (single needle, 10 cm). In all instances, sample quantity was chosen such that the entire needle length was in contact with the sample. Using thermo-gravimetric analysis (TGA, Discovery TGA55, TA Instruments) the thermal stability of the optimized blend and composite were characterized by heating the sample at a rate of 10 °C per minute in a temperature range of 30–300 °C under N_2 gas purging.

2.7. Thermal performance of the OH-64 composite in a temperature-controlled box

To assess the performance of our novel eutectic PCM composite in maintaining adequate temperature control for a thermally sensitive payload against hotter ambient temperatures, a cold-chain transport scenario was simulated by monitoring the temperature of a known weight of Cadbury Bourneville chocolates (payload, Fig. 2b) inside a box constructed with corrugated cardboard and PCM composite-filled pouches (temperature-controlled box, TCB) during exposure to

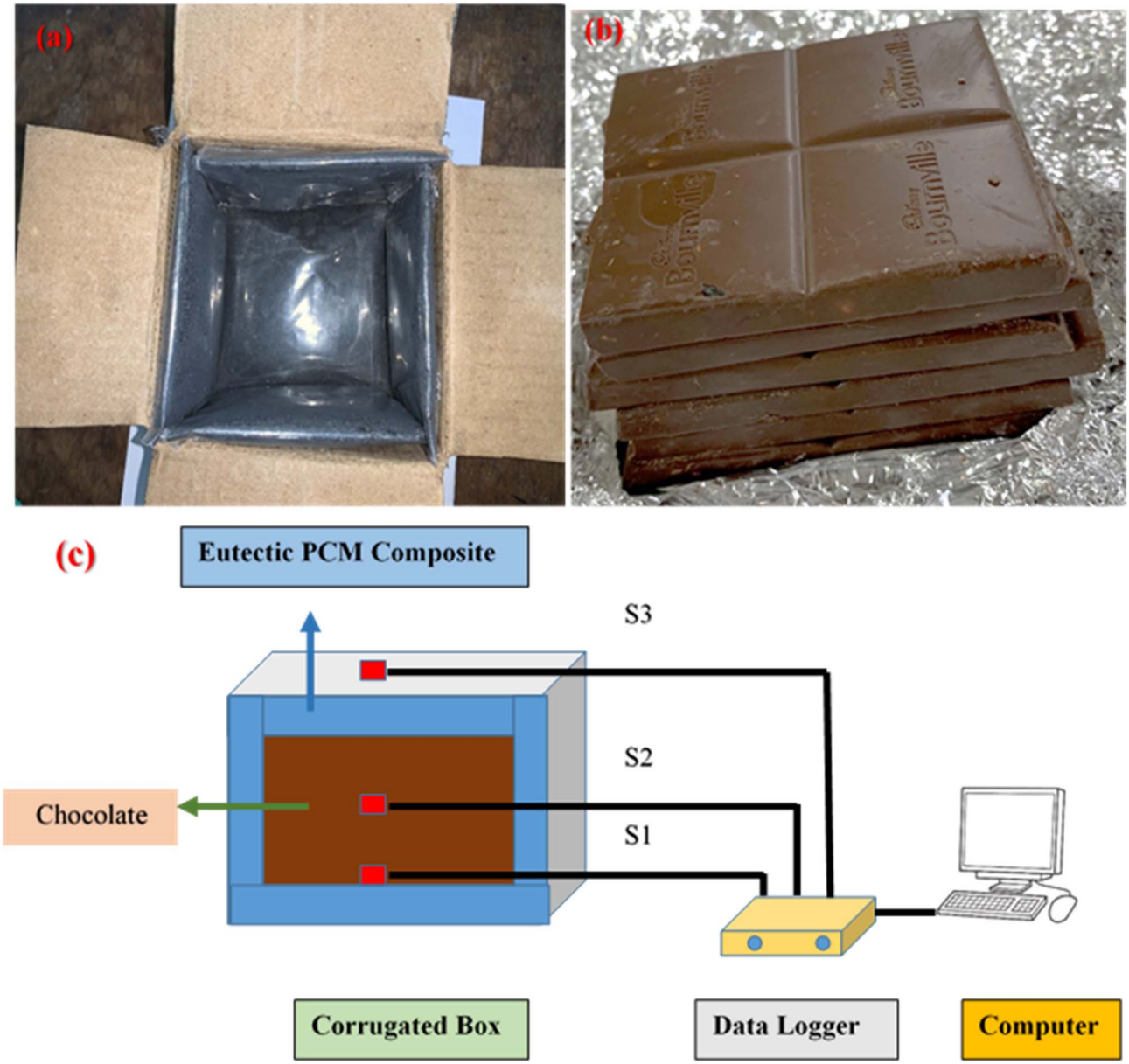

Fig. 2 (a) An inside view of the TCB. (b) A photograph of the chocolate used for the experiments. (c) The experimental set-up for eutectic OH-64 composite application in TCB with 240 g of chocolate.

different outside temperatures. To construct the TCB, 180 g of PCM composite was first filled, uniformly spread (*i.e.*, keeping the mass per unit surface area of the packet constant), and sealed in low-density polythene packets (film thickness: 0.145 mm). Then, six such PCM packets were affixed to, and completely covered, the inner walls of the TCB (outer dimensions ($L \times W \times H$): 12.6 cm × 11.8 cm × 9.1 cm; corrugation thickness 2 mm) to assess the thermal performance of the material (Fig. 2a – photograph and Fig. 2c – schematic illustration of the setup). Three sensors, connected to a temperature data logger (the five-channel data logger machine was equipped with an Arduino Uno, DS18B20 Temperature Sensor, and Micro SD Card Module coded through Arduino IDE), were placed within the TCB to assess the evolution of temperature with time. As seen from Fig. 2c, sensor S1 was placed at the bottom, at the interface of the bottom PCM pouch and payload. Sensor S3 was suspended outside the TCB to record the ambient temperature, while sensor S2 was sandwiched between the chocolate pieces. Once fully assembled, the TCB, was initially stored within a freezer at −14 °C for PCM charging (*i.e.*, solidification) and held there until thermal equilibrium was reached (which was determined from the temperature readings on S1). To better understand the discharging behavior (*i.e.*, the thermal shielding of the payload *via* PCM melting), the activated TCB was subsequently removed from the refrigerator and placed in a convection oven set at temperatures simulating the required ambient conditions, after the payload was introduced in the activated box.

The temperature of the TCB was continuously recorded on a computer using thermocouple sensors to monitor the internal and external temperatures. To preserve the chocolate's distinctive shape, structure and flavor, temperatures must be kept below 25 °C, and therefore, the "backup hours" were defined and calculated as the duration for which sensor S2 registered temperatures below 25 °C from the moment the TCB was placed in a heated oven.

3. Results and discussion

3.1. Morphologies of EG and the eutectic PCM composite

As seen in the FESEM micrographs in Fig. 3, EG has a pronounced worm-like structure with a mesh of pores with sizes between 1 μm and 10 μm fanned out along its curved periphery (Fig. 3a). These pores are mostly absent/hidden in samples containing the OH-64 composite (Fig. 3b). Upon thermal expansion, the chemical moieties intercalated between adjacent graphene sheets quickly and aggressively volatilize into oxidized gases, leaving the graphene sheets substantially cleaved apart in the wake of these "nano-explosions"[50,51] (often heard as crackling/sizzling sounds during the thermal expansion), thus rendering the micrograph seen in Fig. 3a. In this state, each worm of EG resembles a highly lipophilic nanofoam, capable of entrapping the organic PCMs through weak van der Waals's forces and capillary action.[52,53] In other words, the absence of pores and the replacement of the otherwise scaly texture of graphene from Fig. 3a with larger and softer-looking flakes in Fig. 3b demonstrates that PCM has filled and covered all the porous carbonaceous foams. This lends confidence to the assumption that the EG-PCM composite would have improved form and thermal stability, as well as better PCM confinement, and the same is discussed in the forthcoming sections.

3.2. Thermal properties of OM-18, hexadecane, eutectic mixtures, and the OH-64 composite

The melting and crystallization thermograms of various combinations of OM-18 and hexadecane are stated in Fig. 4. For all the samples, the calorimetric runs were scanned in the temperature ranges of −10 °C to 25 °C (heating) and 25 °C to −10 °C (cooling). All samples except OH-64 and OH-73 displayed multiple peaks of melting/freezing in their thermograms. At first glance, the phase change features in both these samples appear similar, although some nuanced observations suggest that OH-64 is an optimal eutectic mixture. Firstly, note the presence of multiple transition features in heating and cooling cycles for all thermograms and their general movement across the temperature axis as the formulation changes. Each peak denotes a phase transition arising from a corresponding single component or a miscible mixture of components, and the eutectic mixture should have a single melting/freezing transition, where the phase transitions of all mixture components are synchronized. In the presented thermograms, on moving from one formulation extremum (OH-19) to another (OH-91), we see a gradual depression of the onset of these transition events (peaks move to lower temperatures), up to OH-64, beyond which the onset of these events starts occurring at higher temperatures. In a similar trend, the multiple melting or freezing events start to converge as we approach OH-64 and OH-73 thermograms, wherein all events of a given phase transition overlap into single peaks. This inflection of thermal behavior with different OM-18/hexadecane ratios is indicative of eutectic behavior in the vicinity of OH-64 and OH-73 mixtures. In OH-73, the transition peaks are comparatively broader and have subtle shoulder-type distortions that are indicative of the partial convergence of multiple transition events. Thus, OH-64, with its distinct and sharp melting/crystallization peak, can be considered a eutectic PCM mixture.

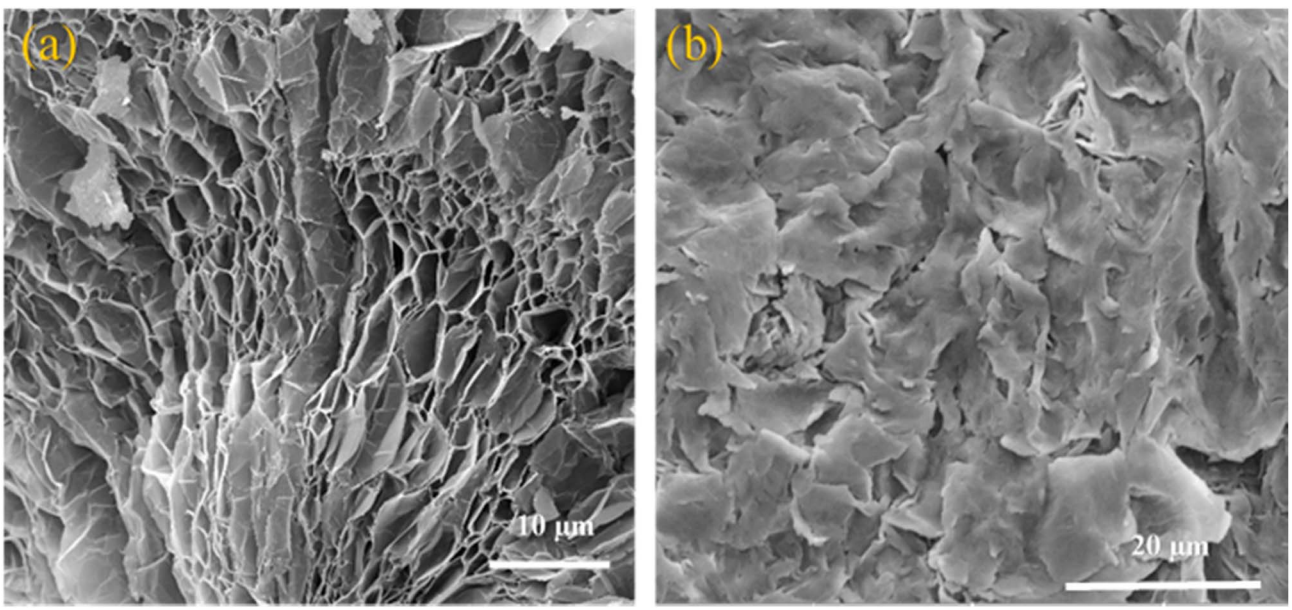

Fig. 3 Microstructure characterization. (a) EG and (b) PCM-EG eutectic composite.

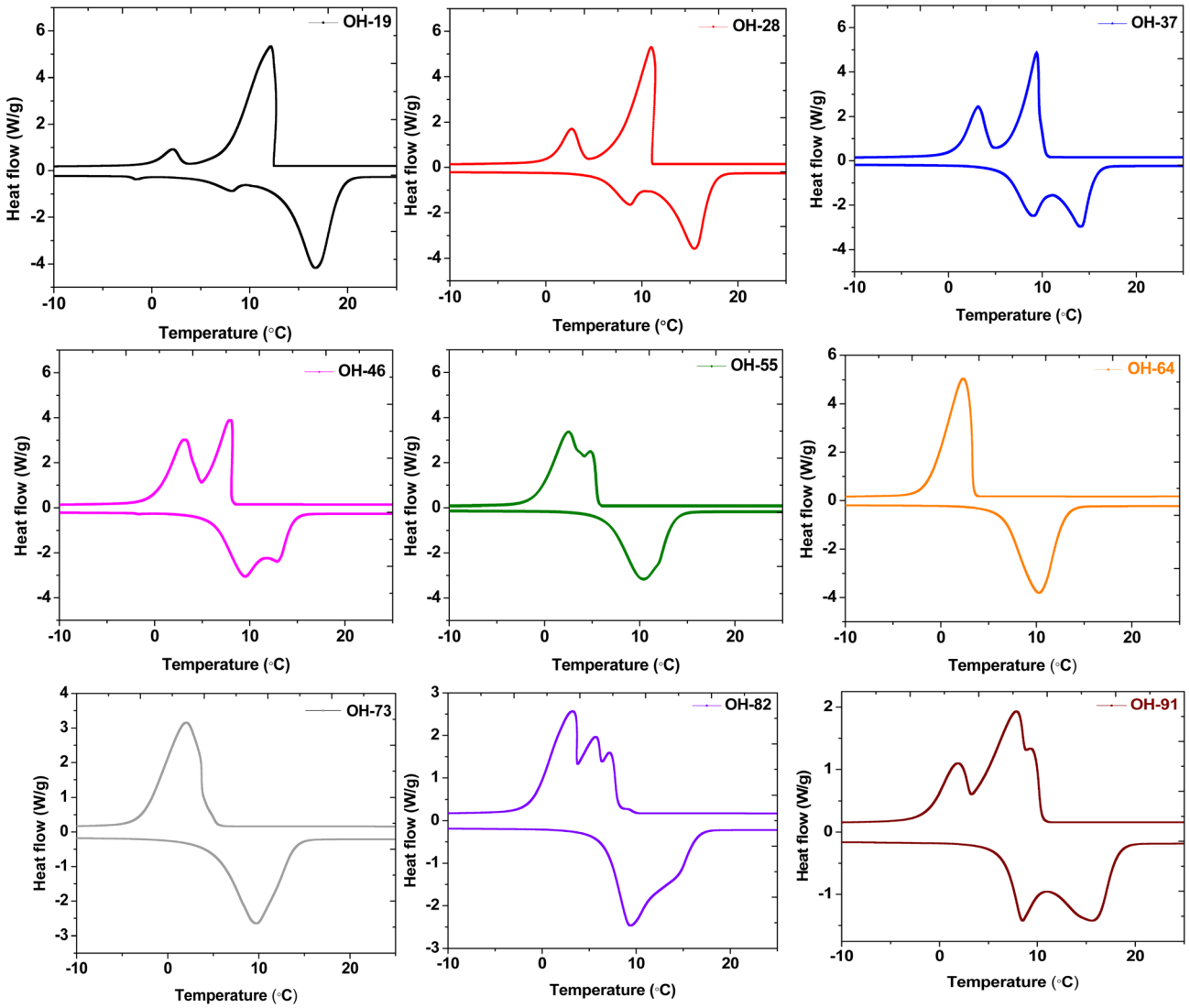

Fig. 4 DSC thermograms of OM-18 and hexadecane mixture samples.

To accurately quantify the thermal properties of the resulting eutectic mixture, DSC runs were repeated on OH-64 with a slow heating/cooling temperature ramp rate of 0.5 °C min^{-1} and isothermal steps of two minutes before each heating/cooling segment in the temperature range of −10 °C to 25 °C. The resulting thermogram is shown in Fig. 5, along with thermograms of the constituent PCMs (OM-18 and hexadecane) under similar testing conditions. The melting temperature of the eutectic OH-64 (deduced from the onset of the endothermic peak in the corresponding thermogram) was 6.87 °C, while the freezing point was noted as 4.86 °C, both values being lower than component PCMs (OM-18: 16.15 °C melting and 16.32 °C freezing, and hexadecane: 17.92 °C melting and 17.15 °C freezing). The enthalpies of melting and freezing for OH-64 were 170.43 kJ kg^{-1} and 170.93 kJ kg^{-1}, respectively.

The thermal properties of the composite prepared by blending exfoliated graphite with OH-64 were evaluated similarly. The prepared OH-64 composite showed melting at 8.86 °C and freezing at 9.17 °C, with corresponding phase change enthalpies of 161.07 kJ kg^{-1} and 159.30 kJ kg^{-1}. Interestingly, compared to OH-64, the latent heat capacity of the OH-64 composite was only reduced by ~5–7%, whereas the PCM content in the composite was reduced by ~11%. These shifts in transition temperatures and anomalous offset in phase change enthalpies upon the incorporation of EG tracks a well-noted trend in previously reported EG-PCM composites[44,48,54] and has been attributed to confinement effects, the reduction of supercooling due to graphite surfaces and the high conductivity of the graphite particles. The DSC thermogram of the OH-64 composite is also shown in Fig. 5, and the thermal properties of OM-18, hexadecane, OH-64, and the OH-64 composite are compiled in Table 2.

According to the principle of the mutual depression of melting points due to the presence of surface energy-reducing impurities, the phase change temperatures of our eutectic

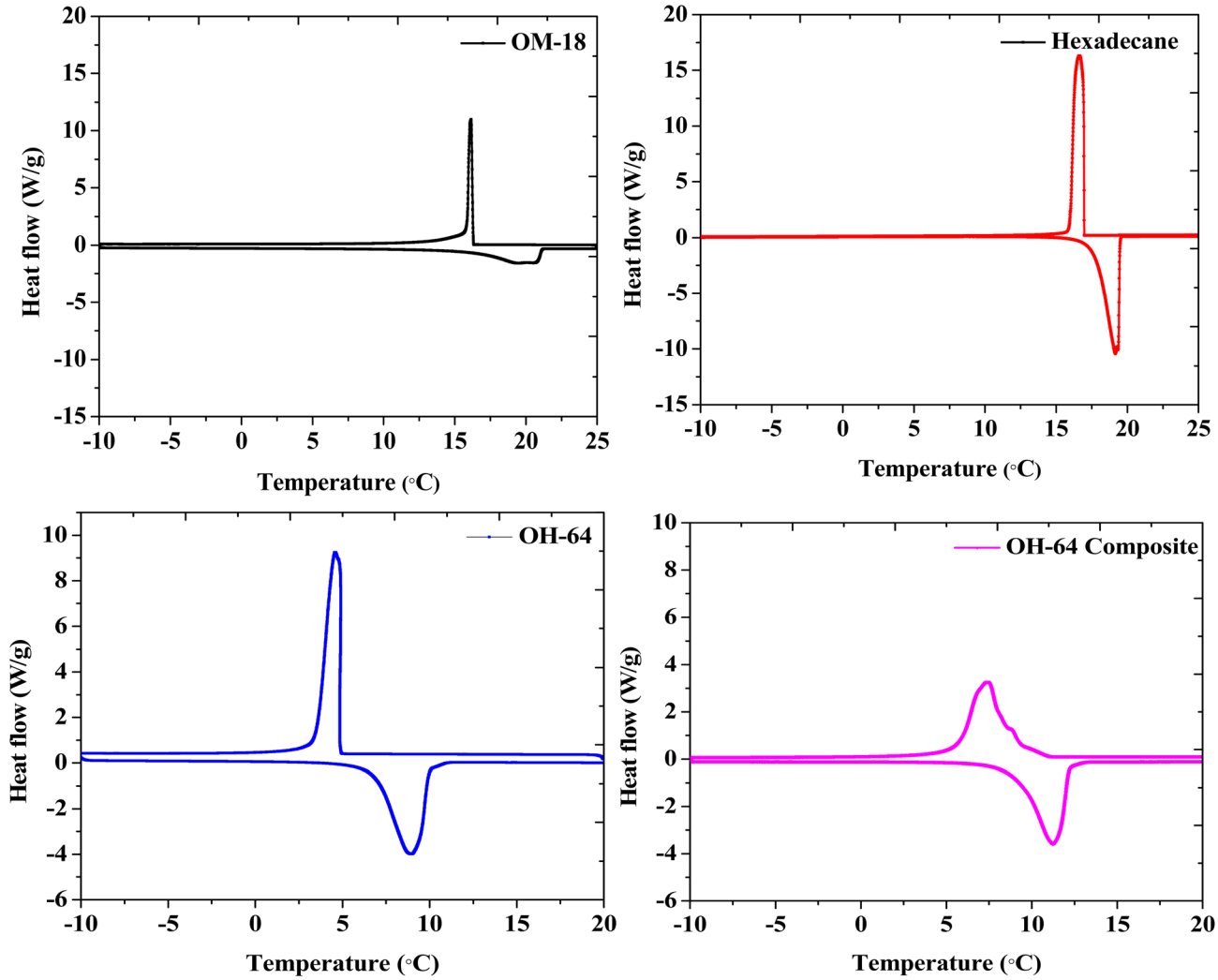

Fig. 5 DSC thermograms of OM-18, hexadecane, OH-64, and the OH-64 composite.

mixture should be lower than those of the individual PCMs. Thus, for a given binary eutectic mixture, we can predict the eutectic composition of OM-18 and hexadecane by using the Schrader equation for binary mixing,[24] with the underlying rationale that each constituent of the mixture acts as a soluble impurity for the other and the eutectic point is achieved at the composition where the resulting effect of melting point depression is equal for both PCMs. Thus, assuming ideal mixing in their liquid states, for both components, the reduction in melting temperatures from their pure compositions to their eutectic point is given by the following:

$$\Delta T_i = T_i^f - T_e^f = \frac{RT_i^f}{\Delta H_i^f} T_i^f (-\ln x_i^e);$$

where ΔT_i = net freezing point depression in component i; T_i^f = freezing point of pure component i; T_e^f = eutectic freezing point; x_i^e = eutectic composition mole fraction of component i; ΔH_i^c = enthalpy of crystallization for component i.

Table 2 Thermal properties of PCMs, eutectic PCM, and the PCM composite

	Melting properties			Crystallization properties		
Sample name	Onset (°C)	Peak (°C)	Enthalpy (J g^{-1})	Onset (°C)	Peak (°C)	Enthalpy (J g^{-1})
OM-18	16.15	19.46	140.72	16.32	16.20	163.85
Hexadecane	17.92	19.38	206.46	17.15	16.20	210.38
OH-64	6.87	8.96	170.43	4.86	4.58	170.93
OH-64 composite	8.86	11.26	161.07	9.17	7.40	159.30

Solving this equation for our binary composition (x^{e}_{OM18} + $x^{e}_{Hexadecane} = 1$), the model predicts a eutectic freezing temperature of *ca.* 4.9 °C at a mass composition of 55% OM-18 and 45% hexadecane (Fig. 6). While not precise, these predictions are quite close to the reported experimental values of the resulting eutectic composition. More curiously, the latent heat capacity as predicted by the model appears to be about 8% higher than values reported from DSC (184.72 kJ kg^{-1} obtained from the calculations *vs.* 170.93 kJ kg^{-1} obtained from DSC results). Further, if we extend our calculations of latent heat capacity to the lab-prepared mixture (60 wt% OM 18 and 40 wt% hexadecane), the resulting value (180.95 kJ kg^{-1}) is still higher by about 6%. We believe that these deviations arise from minor errors in the preparation and characterization of the lab-prepared compositions, as well as the departure of the real samples from the ideality of the Schrader equation. While more work is needed to elucidate the nature of thermodynamic relationships in a eutectic mixture of three or more components, for the current study, we believe that the Schrader equation reasonably validates the experimentally obtained composition showing eutectic behavior.

3.3. Thermal stability

Using thermogravimetric analysis, the thermal stabilities of OM-18, hexadecane, OH-64, and the OH-64 composite were assessed between room temperature and 300 °C. Thermal degradation of all samples showed a one-step process, and the ranges of temperatures in which degradation occurred in the corresponding samples are presented in Table 3. Hexadecane exhibited nearly 100% weight loss between 68 °C and 146 °C, signifying hasty evaporation with temperature. OM-18 started losing weight beyond the temperature of 98 °C and lost most of its weight by the time the temperature reached 185 °C. OM-18 started losing its weight at a higher temperature (98 °C) compared to that of hexadecane (68 °C), which might be caused by the existence of carboxyl groups (–COOH) in OM-18, which decreased volatility due to increased chemical interactions (*e.g.*, hydrogen bonding). Eutectic OH-64 closely followed the thermogravimetric behavior of OM-18 and completely degraded in the temperature range of 97–184 °C. With the incorporation of EG, the degradation onset and endset in this mixture (OH-64 composite) were lowered, and the degradation step spanned between 90 °C and 167 °C. The total weight loss percentage noted with the eutectic OH-64 composite was 87.99%, which matches the theoretical PCM content present in the composite (Fig. 7). Thus, neither the blending of PCMs nor the

Table 3 The weight loss % of PCMs, eutectic PCM, and the PCM composite

Sample name	Weight loss onset temperature (°C)	Weight loss end temperature (°C)
OM-18	98	185
Hexadecane	68	146
OH-64	97	184
OH-64 composite	90	167

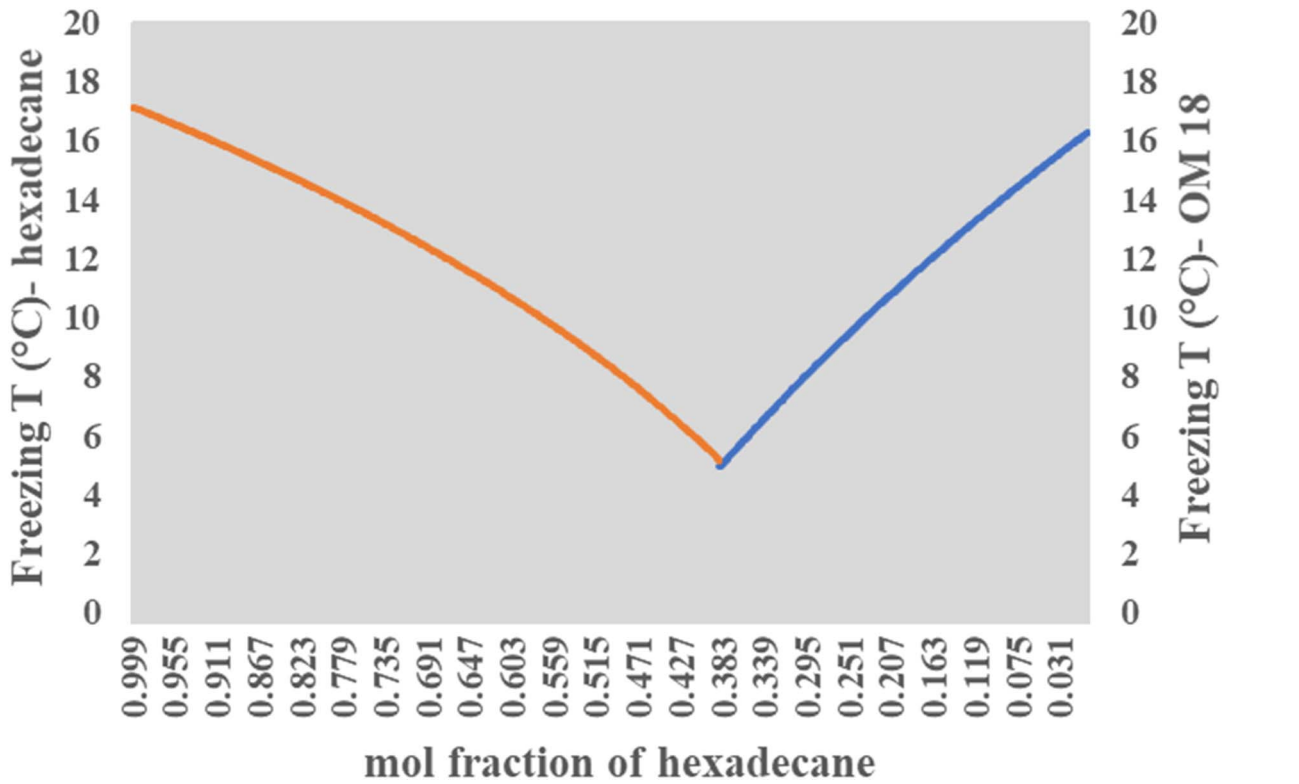

Fig. 6 Plot of the eutectic model based on the Schrader equation.

introduction of EG impacted the thermal stability of the composite, making it a viable and promising material for thermal energy storage. The degradation behaviors of all four materials are presented in Table 3.

By subjecting the sample to numerous thermal cycles, the performance stability of the composite was assessed (heating and cooling). The long-term usefulness of the composite is determined by its thermal stability and performance repeatability under recurrent phase transition. The eutectic PCM composite OH-64 was subjected to 100 full thermal (heating/cooling) cycles, with each cycle consisting of the sample being gradually heated from −10 to 25 °C in the course of the heating cycle and the reverse in the cooling cycle. Fig. 8a shows the DSC thermograms for every 25 cycles up to the 100th cycle, and no significant change in peak temperatures and enthalpy values was immediately visible. Accompanying FESEM images of the composite subjected to 100 cycles also appeared morphologically identical to freshly prepared samples (Fig. 8b). As a result, the PCM composite constructed with EG as a porous support matrix showed good thermal consistency after 100 heat cycles with just a 5% reduction in melting/crystallization enthalpy.

3.4. FTIR-ATR analysis of OM-18, hexadecane, OH-64, and the OH-64 composite

The FTIR-ATR spectra of hexadecane, OM 18, OH-64, and the OH-64 composite were used to tease out the molecular level interactions and changes in the chemistry (if any) of the constituents of the optimized eutectic mixture and composite. Fig. 9 presents all these IR spectra stacked on a common *x*-axis for easy comparison. Twin peaks of medium intensity at around 2900 cm^{-1} and 2825 cm^{-1}, indicative of symmetrical stretching of the –CH_3 and –CH_2 groups[35,37] in the saturated alkyl chains, and typical of many hydrocarbon chains, were observed in both OM-18 and hexadecane. This was expected since both are organic phase change materials. However, in the case of OM-18, these characteristic twin peaks were superimposed atop a broad and subtle peak spanning 3400 cm^{-1} and 2600 cm^{-1}, which is representative of –OH stretching in the carboxylic acid and as such, this feature is absent in the hexadecane spectrum. Similarly, peak doublets at 1453 cm^{-1} and 1398 cm^{-1} (in OM-21), and 1453 cm^{-1} and 1371 cm^{-1} (in hexadecane) exemplify the symmetric and asymmetric bending of methyl moieties that are present in both materials. There are a few other peaks that also suggest the fatty acid composition of OM-18, including a clear and distinct peak at 1703 cm^{-1} originating from the stretching modes in the carbonyl group (–C=O) of the carboxylic acids, and another peak at 703 cm^{-1} denotes in-plane swinging of the carboxylic acid –OH bond,[55] while the peaks at 1260 cm^{-1} and 926 cm^{-1} represent in-plane and out-of-plane bending vibrations in the hydrogen-bonded dimers of the fatty acid molecules.[6] Note that a peak in the vicinity of 700 cm^{-1} (at 713 cm^{-1} precisely) was also seen in the hexadecane spectrum but this is due to the in-plane rocking of the CH_2 groups. Furthermore, the evidence of fatty acid dimerization was present in the peak at 926 cm^{-1} and a shoulder appeared at around 2600 cm^{-1}. Apart from this, there were several smaller peaks identified in the fingerprint region, which may be ascribed to fatty acids; however, since OM-18 itself is an organic fatty acid blend, it is difficult to discern and accurately ascribe these signals to specific functional moieties.

The spectrum of hexadecane has two distinct absorption peaks: one occurred at 713 cm^{-1}, which corresponds to the in-plane rocking vibration of CH_2 groups.

The IR spectrum of the eutectic PCM and the eutectic PCM composite both showed characteristic peaks and while the peak intensities appeared subdued (due to lower activity of constituent moieties), no peak shifts were observed, confirming that OM-18 and hexadecane did not interact chemically. Furthermore, on comparing OH-64 and the OH-64 composite, a non-zero slope/drift was observed in the composite spectrum. This is due to the presence of graphite in the composite, which has no distinctive peaks in the IR spectrum but shows a consistent wavelength-dependent IR absorption behavior.

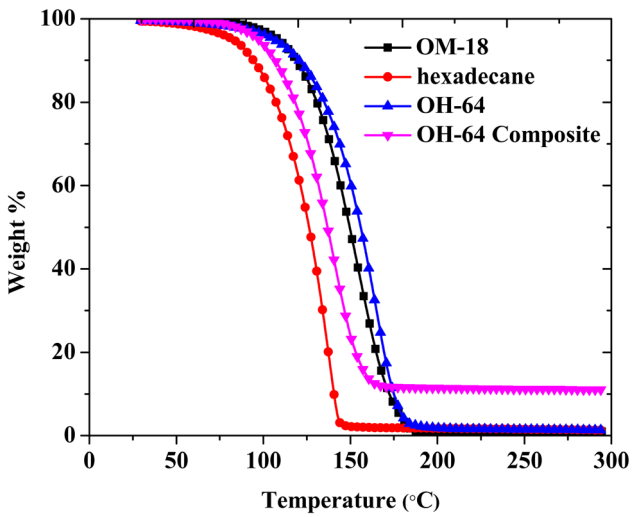

Fig. 7 TGA thermograms of OM-18, hexadecane, OH-64, and the OH-64 composite.

3.5. Application of the OH-64 eutectic composite in a TCB for temperature maintenance of chocolate

The performance of the PCM in cold-chain applications was evaluated by monitoring the thermal control of chocolate bars in a TCB comprising the PCM composite. Chocolate is a temperature-sensitive material that requires a storage temperature below 25 °C to preserve quality. Six packets of OH-64 composite were placed against each side of the TCB, where they were the same laminar size as the inner walls. Before commencing the experiment, 240 g of chocolate was placed as a "payload". Thermocouples S1, S2, and S3 were used to record temperatures at the PCM packet-chocolate interface, within the payload, and the ambient temperature, respectively. The resulting temperature readings are presented in Fig. 10. From the time that the entire setup was subjected to sub-zero temperatures in the refrigerator, it took ~7.8 hours for the chocolate to reach the equilibrium temperature of −14 ± 1 °C (cooling/charging phase). Of note are the change in the slope and the gradual plateauing of the temperature at S1 between 2.5

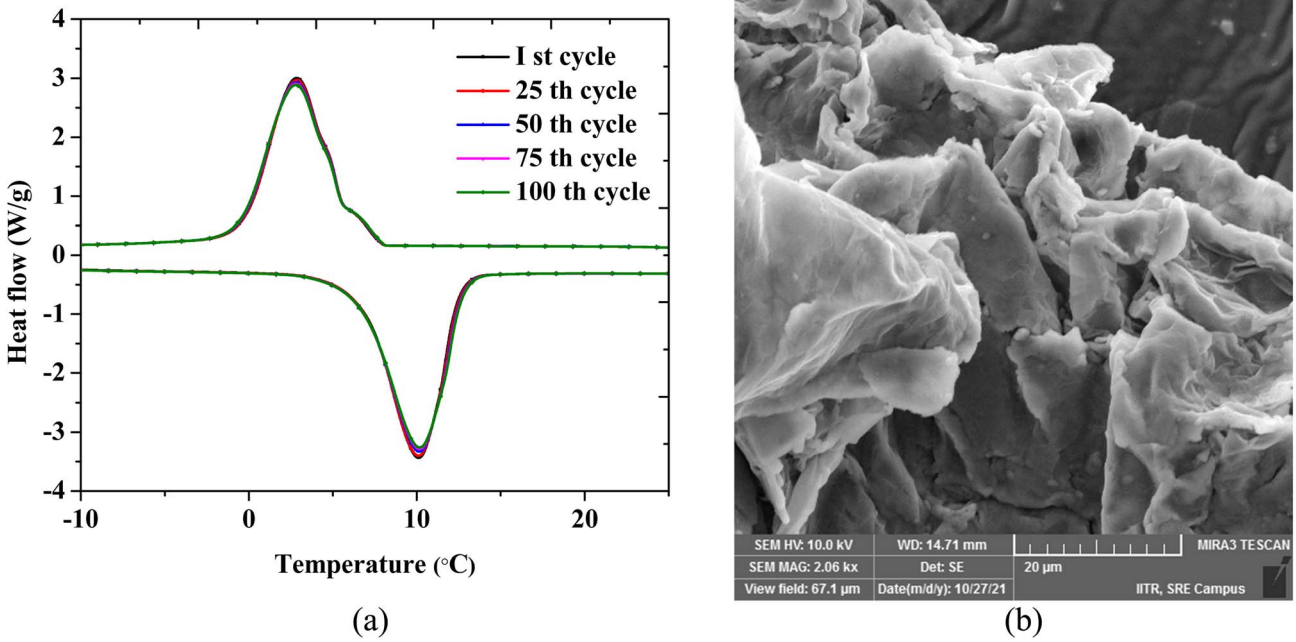

Fig. 8 (a) DSC thermograms of the eutectic PCM composite. (b) A SEM image of the composite after 100 thermal cycles.

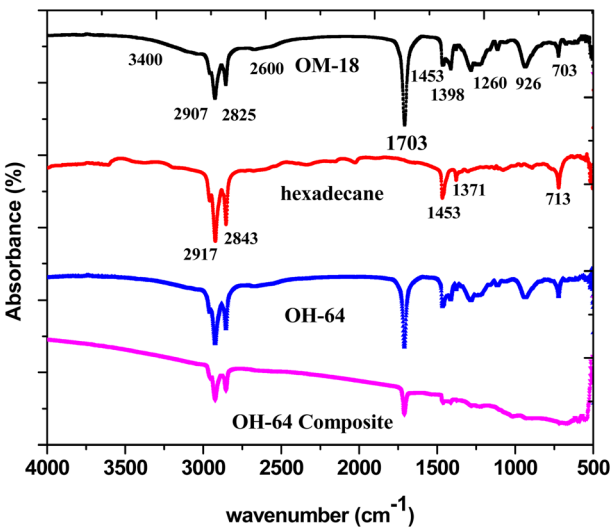

Fig. 9 FT-IR spectra of OM-18, hexadecane, OH-64, and the OH-64 composite.

°C to 10 °C, which indicated the occurrence of the liquid-to-solid phase transformation in the OH-64 composite. As a result, the chocolate's temperature could not be lowered quickly (S2). About 8 hours after initiation, the TCB was removed from the refrigerator and located at an ambient temperature of 31 °C. The temperature of the product started increasing in response to the external conditions but the heat influx was significantly impeded in the same temperature window due to the phase transformation of the composite here as well. The temperature of the chocolate within the TCB stayed below 25 °C for approximately 4.1 hours.

The thermal buffering ability was also checked at outside temperatures of 27 °C and 41 °C. The thermal buffering time (time to maintain the chocolate temperature below 25 °C) was found to be ~5.5 hours and ~2.4 hours, respectively. Thus, as expected, we saw a reduction in the buffering ability of the TCB with an increase in temperature due to increased heat fluxes. Overall, the thermal buffering times for three different ambient temperatures (27, 31, 41 °C) were found to be, respectively, 5.54 h, 4.08 h, and 2.41 h (Fig. 11a).

An equivalent set of experiments was performed with TCB setups where only EG (no OH-64) pouches were included along the walls of the corrugated box, with everything else being

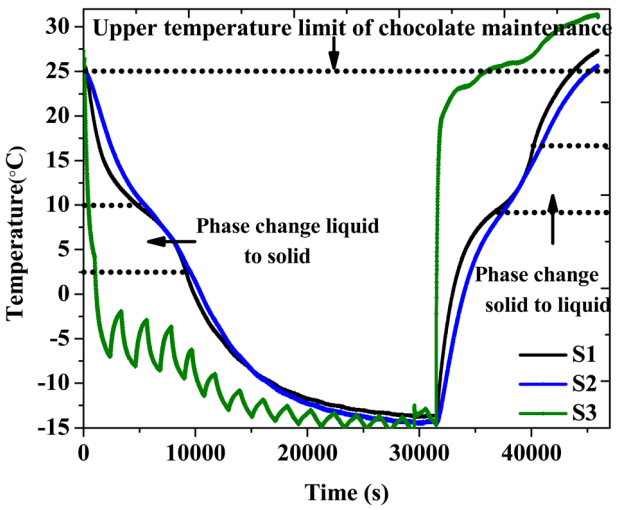

Fig. 10 The charging and discharging profiles of the TCB that included chocolate and the OH-64 composite.

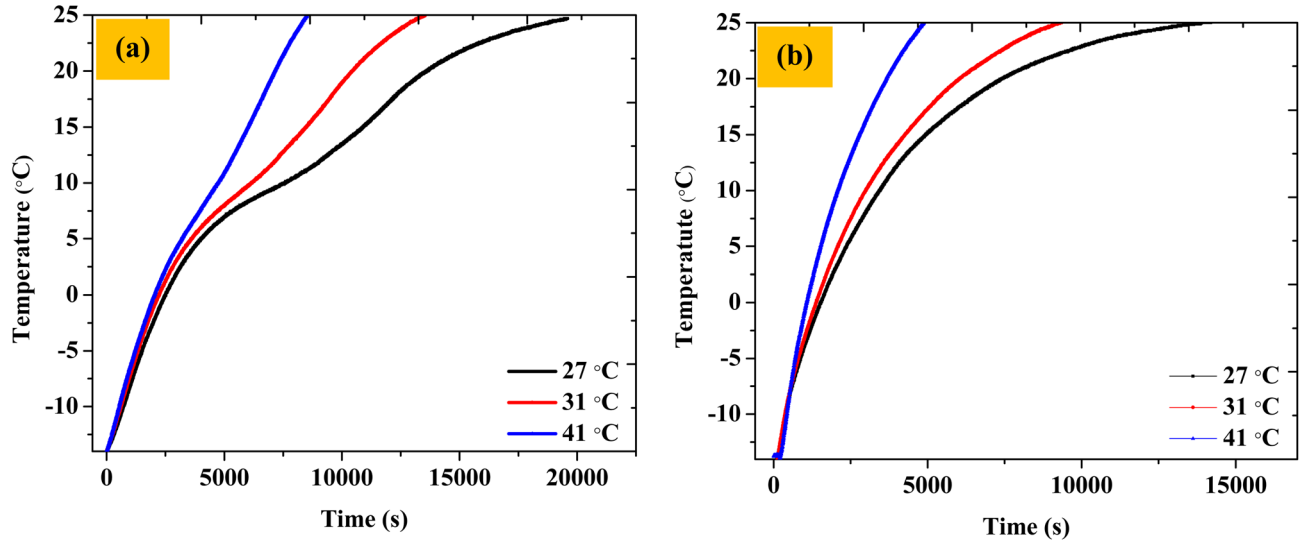

Fig. 11 The temperature of the chocolate when the TCB was exposed to outside temperatures of 27, 31, and 41 °C (a) with the PCM composite and (b) with only EG (without PCM).

identical. This was done to illustrate the efficacy of the PCM material in slowing down the temperature incursions in the 2–10 °C window. As expected, the thermal buffering time (time to maintain the chocolate temperature below 25 °C) was found to be diminished by approximately 33–46% for temperature incursions of 27–41 °C, respectively, compared to TCBs containing PCM (~3.7 h, ~2.6 h, and ~1.3 h as compared to ~5.5 h, ~4.1 h, and ~2.4 h). The OH-64 composite showed enhanced performance as compared to only EG because of the presence of the phase change material. Further, the deterioration in the performance of the TCB upon PCM removal was greater at higher ambient temperature conditions. Thus, the payload approached 25 °C at a 33% faster rate without PCM against an ambient of 27 °C, and the time taken for the payload to achieve the same temperature against an ambient temperature of 41 °C was 46% shorter as compared to the PCM box, underscoring the efficacy of PCM in the TCB (Fig. 11b).

It is noteworthy that despite the improvement in the thermal sensitivity of the payload due to the presence of the EG-PCM composite, the thermal buffering times reported are not pragmatic for any real cold chain applications (most cold chain applications commonly require 6–8 hours of continuous thermal control for safe transport, well above the 5.5 hours reported for a relatively cool 27 °C environment in this study). While increasing the PCM quantity is expected to result in improved buffering times, the absence of any insulating material within the system is the primary reason for the low thermal buffering times. In the absence of an insulating material, the PCM discharges not only to compensate for temperature incursions against the payload but also against the ambient temperature, and a strategic combination of PCM and insulating materials is usually required in designing PCM-based TCBs.

Interestingly, the granular form factor of the OH-64 composite does impart insulating properties to the PCM for these applications due to the presence of significant air pockets between the PCM grains; however, this reduction in thermal conductivity is almost completely offset by the presence of highly thermally conductive graphite in the composite matrix. Table 4 lists the thermal conductivity values obtained for OH-64 and the OH-64 composite when the incorporated PCMs were frozen and molten. The enhancement of the thermal conductivity of any material by the incorporation of graphite and exfoliated graphite as a filler is well noted in several reports.[44,48,54] In the case of OH-64, at first glance, the thermal conductivity of the PCM and EG-incorporated PCM are very similar, with arguably minor improvements seen for liquid phase thermal conductivity. This composite exhibited a bulk density of approximately 0.4 g cm^3, and when compressed to

Table 4 Thermal conductivity of OH-64 and OH-64 composites at different temperatures and densities

Sample	Temperature (°C)	Thermal conductivity (W m^{-1} K^{-1})	Bulk density (g cm^3)
OH-64	20	0.148 ± 0.004	—
	−27	0.205 ± 0.007	
OH-64 composite	20	0.199 ± 0.010	0.395
	−16	0.168 ± 0.005	
OH-64 composite compressed	24	1.946 ± 0.034	0.784
	−24	1.013 ± 0.030	

double the bulk density ($\approx$0.8 g cm^3), the thermal conductivity increased by almost 900% in the liquid state and by about 500% in the solid state (note: liquid and solid states indicate the phase of the PCM entrapped within the exfoliated graphite; the composite itself remains solid throughout the operable temperature range). These results reflect the fortuitous benefit of preparing PCM composites for cold chain solutions in this manner, where the granularity of the PCM material may be leveraged and tuned to provide tailored thermal insulation properties in addition to the thermal buffering properties from the PCM itself.

4. Conclusions

Using the blending ultrasonication process, eutectic PCM was developed using the OM-18 commercial fatty acid combination and hexadecane.

(1) Experimental evaluation revealed that the special mixture that produced the eutectic PCM (OH-64) has 60 wt% OM-18 and 40 wt% hexadecane.

(2) The shape-stabilized composite was prepared by the impregnation of the OH-64 eutectic PCM into the supporting matrix EG, and the leakage test confirmed that the maximum loading capacity of PCM was 88.9 wt%.

(3) The melting temperature of the OH-64 eutectic composite was 8.86 °C, and the latent heat of melting was 161.07 kJ kg^{-1}.

(4) The IR spectra of the eutectic PCM and eutectic PCM composite showed characteristic peaks for both PCMs with no peak shifting problems, confirming that OM-18 and hexadecane did not interact chemically.

(5) When the eutectic OD-64 composite was subjected to a TGA examination, it was discovered to be thermally stable up to 90 °C but began to lose weight after that.

(6) After 100 heat/cool cycles, the OH-64 composite demonstrated decent thermal cycling stability with no significant changes in the melting and crystallization temperatures and just a 5% loss in melting and crystallization enthalpy.

(7) The PCM composite exhibited a bulk density-dependent thermal conductivity, where doubling the bulk density of the OH 64 composite powder resulted in the thermal conductivity of the composite increasing by almost 900% in the liquid state and by about 500% in the solid state.

(8) The time required for chocolate to reach 25 °C using the TCB was determined to be 5.54 h, 4.08 h, and 2.41 h, respectively, once the fully charged TCB holding 240 g of chocolate was exposed to three different outer temperatures, *i.e.*, 27 °C, 31 °C, and 41 °C. As a result, the eutectic OH-64 composite will work well in the TCB to maintain the temperature of heat-sensitive goods.

Thus, in the present work, a new eutectic mixture in the temperature range suitable to cold-chain applications was developed, and its viability for the passive preservation of thermally sensitive transport materials has been demonstrated using a temperature-controlled box assembled in-house. Further, the efficacy of exfoliated graphite in encapsulating the liquid eutectic PCM was found to be excellent, and an otherwise unexplored feature of tuning the thermal conductivity of such a powdered composite by varying the bulk density of the material was brought to light. While straightforward, the preliminary results surrounding this material's seemingly tunable thermal conductivity are of note because of the ability to tailor the material at the meso- and macro-scales to achieve the desired heat transfer properties in real-time. This idea unravels a new perspective in playing with the granularity of these sticky EG for encapsulating phase change materials, and opportunities to create thermo-responsive PCM composites, such as the following: (a) modification of the EG surface chemistries/charges, (b) addition of stimuli-responsive materials as interstitial layers in the EG particles, and (c) changing the particle size distribution and exfoliation/expansion ratio of the particles; these are some of the many ideas that deserve further exploration in future research.

Conflicts of interest

The authors declare no conflict of interest.

Acknowledgements

Financial support to execute the experimental work is gratefully acknowledged to MHRD (Ministry of Human Resources Development) Plan grant (2019-20) and IIT Roorkee (No. OH-35-71-142), IIT Roorkee, India.

References

1 D. J. A. Crommelin, D. B. Volkin, K. H. Hoogendoorn, A. S. Lubiniecki and W. Jiskoot, *J. Pharm. Sci.*, 2021, **110**, 627–634.
2 P. Dixit, A. Konala, V. Jagadeeswara, J. Singh, A. Dasari and S. Chattopadhyay, *J. Mol. Liq.*, 2022, **363**, 119829.
3 N. Lin, C. Li, D. Zhang, Y. Li and J. Chen, *Sustain. Energy Technol. Assess.*, 2021, **48**, 101596.
4 B. Nie, J. Chen, Z. Du, Y. Li, T. Zhang, L. Cong, B. Zou and Y. Ding, *Journal of Energy Storage*, 2021, **40**, 102707.
5 J. R. Vennapusa, A. Konala, P. Dixit and S. Chattopadhyay, *Mater. Chem. Phys.*, 2020, **253**, 123453.
6 V. Jagadeeswara Reddy, K. Akhila, P. Dixit, J. Singh, S. Parvate and S. Chattopadhyay, *Journal of Energy Storage*, 2021, **38**, 102499.
7 J. Du, B. Nie, Y. Zhang, Z. Du, L. Wang and Y. Ding, *Journal of Energy Storage*, 2020, **28**, 101238.
8 P. Dixit, J. R. Vennapusa, S. Parvate, J. Singh, A. Dasari and S. Chattopadhyay, *Energy Fuels*, 2021, **35**, 2704–2716.
9 Y. Zhao, X. Zhang, X. Xu and S. Zhang, *J. Mol. Liq.*, 2020, **319**, 114360.
10 R. Agrawal, K. D. P. Singh and R. K. Sharma, *Int. J. Energy Res.*, 2022, **46**, 6562–6576.
11 P. Dixit, S. Parvate, V. Jagadeeswara, J. Singh, T. Kanti, A. Dasari and S. Chattopadhyay, *Journal of Energy Storage*, 2022, **55**, 105491.
12 J. Singh, S. Parvate, P. Dixit and S. Chattopadhyay, *Energy Fuels*, 2020, **34**, 8919–8930.

13 M. Mehrali, J. E. ten Elshof, M. Shahi and A. Mahmoudi, *Chem. Eng. J.*, 2021, **405**, 126624.
14 X. Li, Y. Zhao, X. Min, J. Xiao, X. Wu, R. Mi, Y. Liu, Z. Huang and M. Fang, *Energy Build*, 2022, **273**, 112384.
15 X. Zhang, L. Guo, J. Ren and X. Kong, *Appl. Therm. Eng.*, 2022, **215**, 118938.
16 S. Li, S. Lin, Z. Ling, X. Fang and Z. Zhang, *Ind. Eng. Chem. Res.*, 2020, **59**, 6751–6760.
17 P. Singh, R. K. Sharma, A. K. Ansu, R. Goyal, A. Sarı and V. V. Tyagi, *Sol. Energy Mater. Sol. Cells*, 2021, **223**, 110955.
18 H. Nazir, M. Batool, M. Ali and A. M. Kannan, *Appl. Therm. Eng.*, 2018, **142**, 466–475.
19 F. Liu, L. Zargarzadeh, H. J. Chung and J. A. W. Elliott, *J. Phys. Chem. B*, 2017, **121**, 9452–9462.
20 Y. Liu and Y. Yang, *Appl. Therm. Eng.*, 2017, **112**, 606–609.
21 V. Chinnasamy and S. Appukuttan, *Energy Storage*, 2019, **1**, 1–9.
22 K. Karthikeyan, V. Mariappan, P. Kalidoss, R. Anish, P. Sarafoji, J. Venkatanageswara Reddy and T. Kumar Satpathy, *Mater. Lett.*, 2022, **328**, 133086.
23 Y. Wang, J. Sui and Z. Xu, *Energy*, 2022, **259**, 125036.
24 C. Xu, W. Wang, H. Zhang and G. Fang, *Thermochim. Acta*, 2022, **715**, 179300.
25 Z. Fan, Y. Zhao, X. Liu, Y. Shi and D. Jiang, *Journal of Energy Storage*, 2022, **53**, 105136.
26 X. Liu, Y. Zhao, Z. Fan, Y. Shi and D. Jiang, *RSC Adv.*, 2022, **12**, 23860–23868.
27 I. Baskar, M. Chellapandian and K. Jeyasubramanian, *Constr. Build. Mater.*, 2022, **338**, 127663.
28 A. Sarı, G. Hekimoğlu, Y. Karabayır, R. K. Sharma, H. Arslanoğlu, O. Gencel and V. V. Tyagi, *Energy*, 2022, **247**, 123501.
29 R. Ye, H. Jiang, J. Wang, X. Yang and X. Shu, *Sol. Energy Mater. Sol. Cells*, 2022, **238**, 111584.
30 P. Dixit, V. J. Reddy, A. Dasari and S. Chattopadhyay, *Journal of Energy Storage*, 2022, **52**, 104804.
31 J. Singh, J. R. Vennapusa, P. Dixit and T. K. Maiti, *J. Taiwan Inst. Chem. Eng.*, 2022, **138**, 104497.
32 P. Dixit, V. J. Reddy, S. Parvate, A. Balwani, J. Singh, T. K. Maiti, A. Dasari and S. Chattopadhyay, *Journal of Energy Storage*, 2022, **51**, 104360.
33 J. Singh, S. Parvate, J. R. Vennapusa, T. K. Maiti, P. Dixit and S. Chattopadhyay, *Journal of Energy Storage*, 2022, **49**, 104089.
34 V. J. Reddy, P. Dixit, J. Singh and S. Chattopadhyay, *Carbohydr. Polym.*, 2022, **294**, 119786.
35 S. Parvate, J. Singh, J. Reddy Vennapusa, P. Dixit and S. Chattopadhyay, *J. Ind. Eng. Chem.*, 2021, **102**, 69–85.
36 X. Min, M. Fang, Z. Huang, Y. Liu, Y. Huang, R. Wen, T. Qian and X. Wu, *Sci. Rep.*, 2015, **5**, 1–11.
37 S. Parvate, J. Singh, P. Dixit, J. R. Vennapusa, T. K. Maiti and S. Chattopadhyay, *ACS Appl. Polym. Mater.*, 2021, **3**, 1866–1879.
38 J. Ji, Y. Wang, X. Lin, B. Liu and X. Zhang, *Journal of Energy Storage*, 2021, **44**, 103256.
39 Y. Zhao, X. Min, Z. Huang, Y. Liu, X. Wu and M. Fang, *Energy Build*, 2018, **158**, 1049–1062.
40 Y. Zhao, B. Sun, P. Du, X. Min, Z. Huang, Y. Liu, X. Wu and M. Fang, *Mater. Res. Express*, 2019, **6**, 10.
41 F. Cheng, X. Zhang, R. Wen, Z. Huang, M. Fang, Y. Liu, X. Wu and X. Min, *Appl. Therm. Eng.*, 2019, **156**, 653–659.
42 Y. Song, N. Zhang, Y. Jing, X. Cao, Y. Yuan and F. Haghighat, *Energy*, 2019, **189**, 116175.
43 Y. Li, X. Zhang, J. M. Munyalo, Z. Tian and J. Ji, *J. Mol. Liq.*, 2019, **277**, 577–583.
44 C. Li, B. Zhang, B. Xie, X. Zhao and J. Chen, *Energy Convers. Manage.*, 2020, **208**, 112586.
45 S. Zhou, Y. Zhou, Z. Ling, Z. Zhang and X. Fang, *Appl. Therm. Eng.*, 2018, **133**, 446–451.
46 A. H. Alkhazaleh, W. Almanaseer, M. Ismail, S. Almashaqbeh and M. M. Farid, *Journal of Energy Storage*, 2022, **50**, 104547.
47 L. Liu, X. Zhang, X. Xu, X. Lin, Y. Zhao, L. Zou, Y. Wu and H. Zheng, *Renewable Energy*, 2021, **179**, 2348–2358.
48 W. Du, H. Fei, Y. Pan, Q. He, J. Zhou and X. Liang, *Constr. Build. Mater.*, 2022, **320**, 126309.
49 J. Liu, D. Jiang, H. Fei, Y. Xu, Z. Zeng and W. Ye, *Mater. Today Commun.*, 2022, **31**, 103325.
50 Y. Yao, Y. Cui and Z. Deng, *RSC Adv.*, 2022, **12**, 17217–17227.
51 S. Wu, T. Li, M. Wu, J. Xu, Y. Hu, J. Chao, T. Yan and R. Wang, *J. Mater. Chem. A*, 2020, **8**, 20011–20020.
52 Z. Yin, Z. Huang, R. Wen, X. Zhang, B. Tan, Y. Liu, X. Wu and M. Fang, *RSC Adv.*, 2016, **6**, 95085–95091.
53 C. Ao, S. Yan, S. Zhao, W. Hu, L. Zhao and Y. Wu, *Energy Reports*, 2022, **8**, 4834–4843.
54 L. Zhao, M. Li, Q. Yu, Y. Zhang, G. Li and Y. Huang, *J. Mol. Liq.*, 2021, **322**, 114948.
55 Y. chao Wan, Y. Chen, Z. xing Cui, H. Ding, S. feng Gao, Z. Han and J. kai Gao, *Sci. Rep.*, 2019, **9**, 1–10.